Supporting information for

Electroreduction of Carbon Dioxide into Selective Hydrocarbons at Low Overpotential Using Isomorphic Atomic Substitution in Copper Oxide

Subramanian Nellaiappan,[†] Ritesh Kumar,[‡] C. Shivakumara,[§] Silvia Irusta,[‖] Jordan A. Hachtel,[⊥] Juan-Carlos Idrobo,[⊥] Abhishek K. Singh,[‡] Chandra Sekhar Tiwary,[#] and Sudhanshu Sharma[*,†]

[†]Department of Chemistry, Indian Institute of Technology Gandhinagar, Palaj, Gandhinagar 382355, Gujarat, India

[‡]Materials Research Center and §Solid State and Structural Chemistry Unit, Indian Institute of Science, Bangalore 560012, India

[‖] Department of Chemical Engineering, Nanoscience Institute of Aragon (INA), University of Zaragoza, Zaragoza 50018, Spain

[⊥]Center for Nanophase Materials Sciences, Oak Ridge National Laboratory, Oak Ridge, Tennessee 37830, United States

[#]Metallurgical and Materials Engineering, Indian Institute of Technology, Kharagpur 600036, India

* E-mail: ssharma@iitgn.ac.in

Number of pages : 21

Number of Figures : 16

Number of Tables : 06

Figure S1

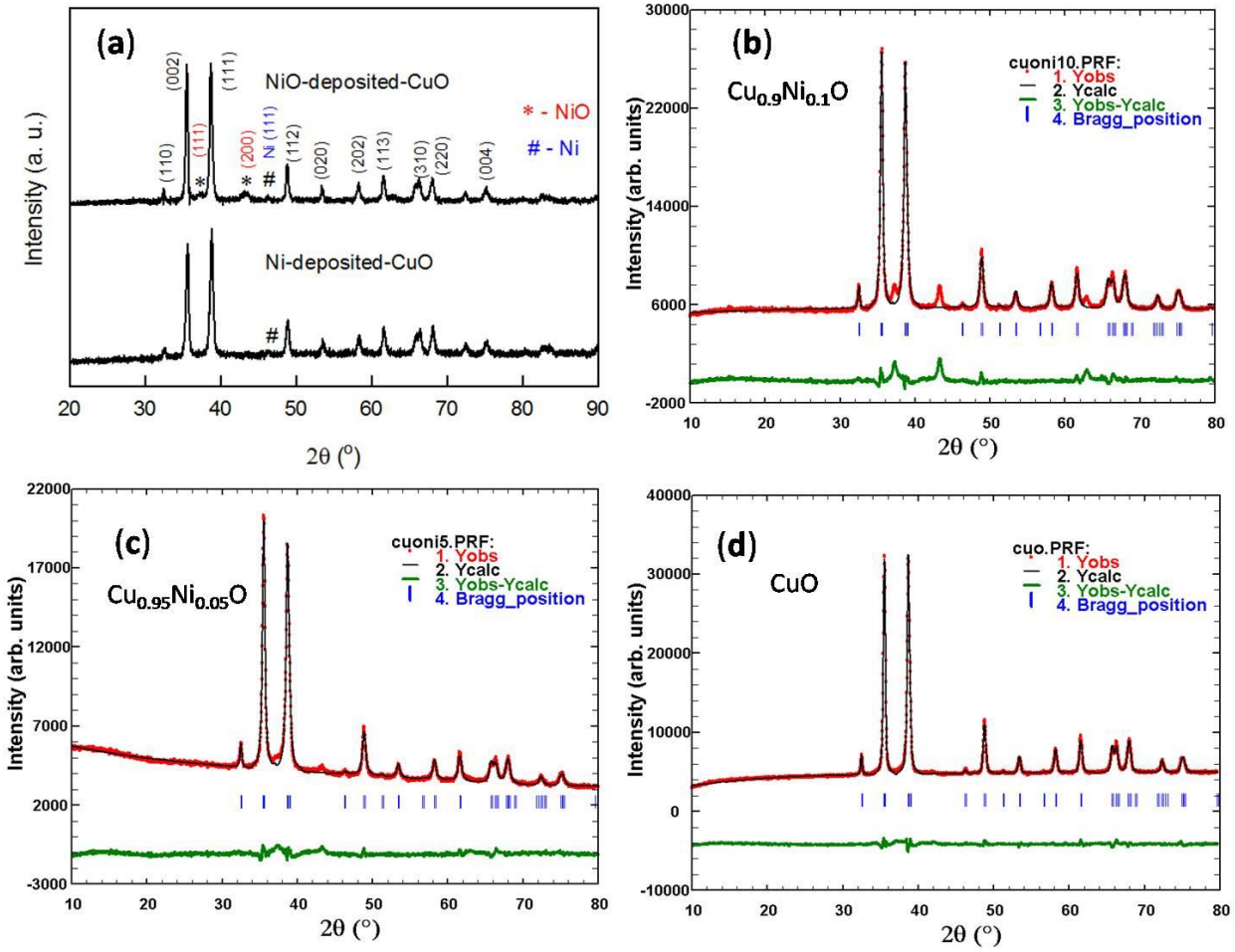

Figure S1. Comparative XRD of NiO and Ni deposited CuO catalysts (a). Rietveld refined observed (Y_{obs}), calculated (Y_{calc}), and difference ($Y_{obs} - Y_{calc}$) XRD patterns of $Cu_{0.9}Ni_{0.1}O$ (b), $Cu_{0.95}Ni_{0.05}O$ (c) and CuO (d); "|" represents the Bragg position.

Figure S2

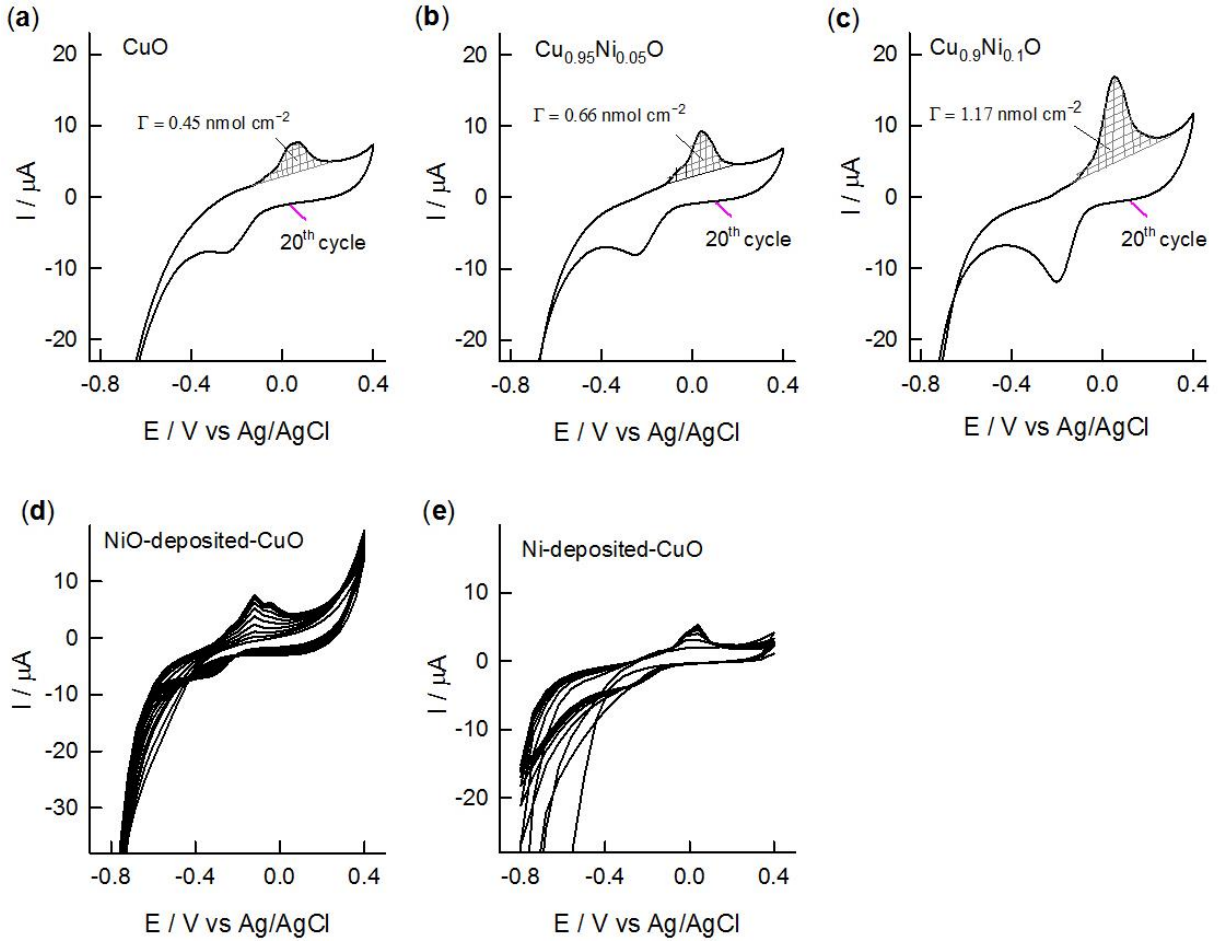

Figure S2. The last CV cycle with their respective calculated surface excess values of CuO (a) $Cu_{0.95}Ni_{0.05}O$ (b) and $Cu_{0.9}Ni_{0.1}O$ (c), Continuous CV responses of NiO-deposited-CuO (d) and Ni metal-deposited-CuO (e) coated GCE at a scan rate of 40 mV s^{-1} in 0.5 M $NaHCO_3$ electrolyte solution.

Figure S3

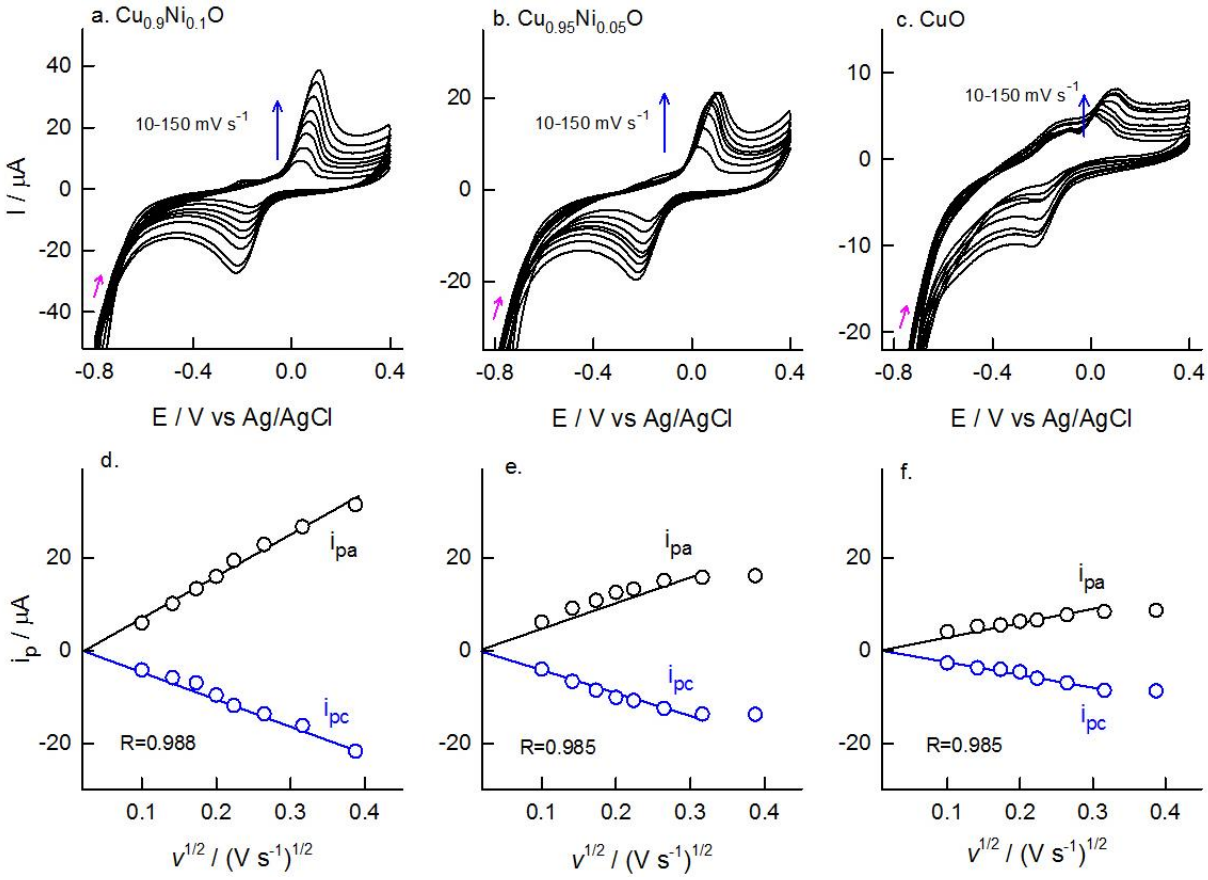

Figure S3. Effect of various CV scan rates from 10 to 150 mV s^{-1} on $Cu_{0.9}Ni_{0.1}O$ (a), $Cu_{0.95}Ni_{0.05}O$ (b) and CuO (c) coated GCE in 0.5 M $NaHCO_3$ electrolyte solution. Corresponding peak current (i_p) versus square root of scan rate ($v^{1/2}$) plots of $Cu_{0.9}Ni_{0.1}O$ (d), $Cu_{0.95}Ni_{0.05}O$ (e) and CuO (f)

Figure S4

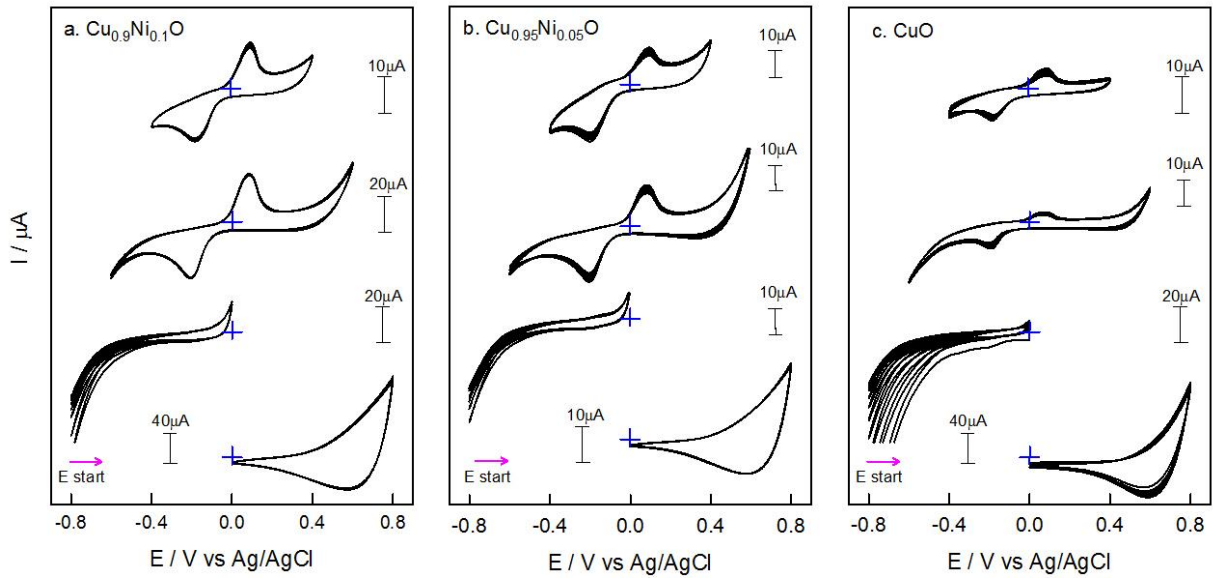

Figure S4. Effect of CV potential windows on $Cu_{0.9}Ni_{0.1}O$ (a), $Cu_{0.95}Ni_{0.05}O$ (b) and CuO (c) coated GCE in various ranges from -0.4 to 0.4 V, -0.6 to 0.6 V, 0 to -0.8 V and 0 to 0.8 V at a scan rate of 40 mV s^{-1} in 0.5 M $NaHCO_3$ electrolyte solution.

Figure S5

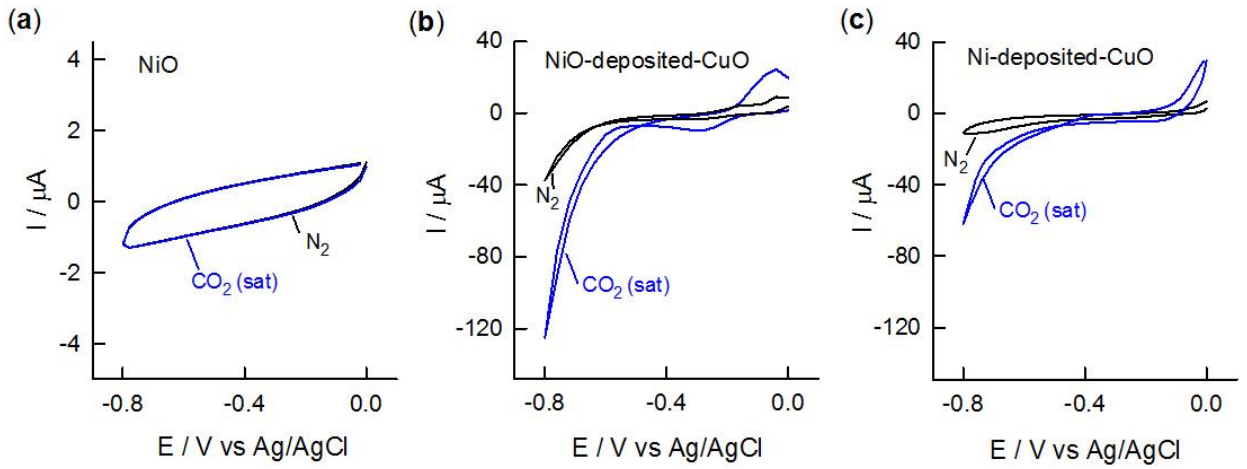

Figure S5. CV response for the electroreduction of CO_2 (saturated for 30 mins) on NiO (a) and NiO-deposited-CuO (b) and Ni-deposited-CuO (c) coated GCE at a scan rate of 20 mV s^{-1} in 0.5 M $NaHCO_3$ electrolyte solution.

Figure S6

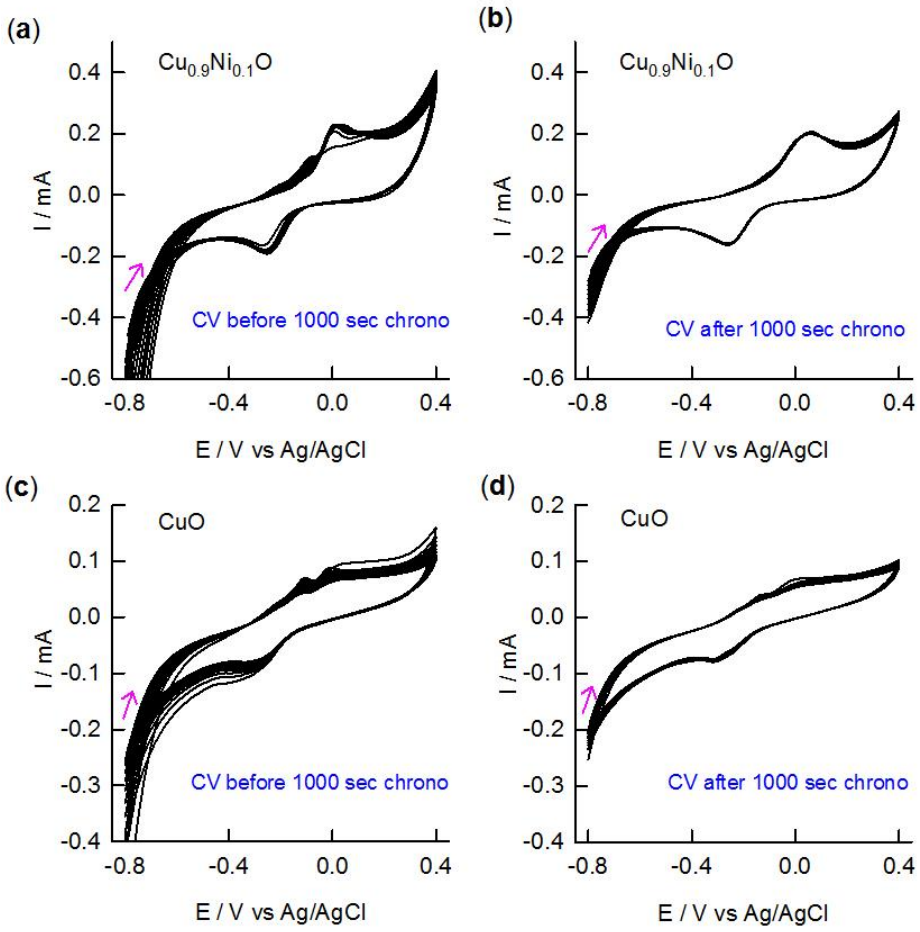

Figure S6. Continuous CV responses of $Cu_{0.9}Ni_{0.1}O$ (a, b) and CuO (c, d) coated GCE in 0.5 M $NaHCO_3$ electrolyte solution (a, c) and after 1000 sec chronoamperometric experiment at -0.8 V in CO_2 saturated 0.5 M $NaHCO_3$ electrolyte solution (b, d) at a scan rate of 40 mV s^{-1}.

Figure S7

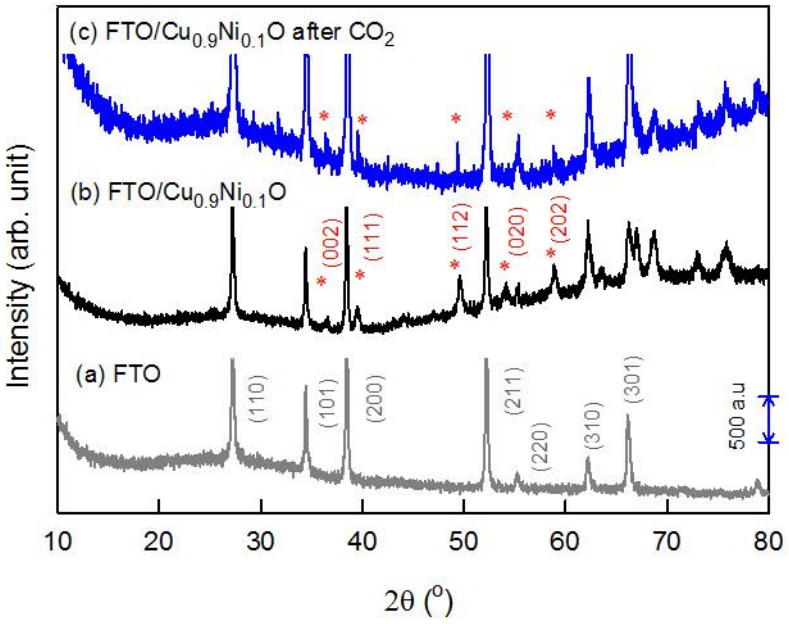

Figure S7. Comparative XRD of bare FTO (a), $Cu_{0.9}Ni_{0.1}O$ coated FTO before (b) and after 1000 sec chronoamperometric CO_2 electrocatalysis (c).

Figure S8

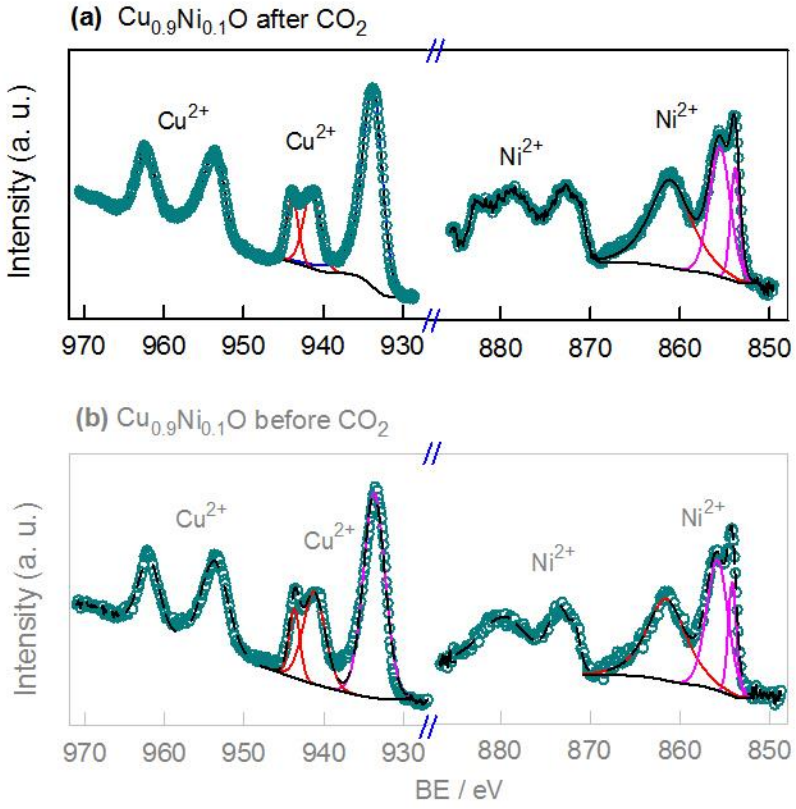

Figure S8. Comparative high resolution XPS Cu(2p) and Ni(2p) spectra of $Cu_{0.9}Ni_{0.1}O$ after 1000 sec chronoamperometric CO_2 electrocatalysis (a) and replicate XPS spectra of as-prepared $Cu_{0.9}Ni_{0.1}O$ catalyst (b).

Figure S9

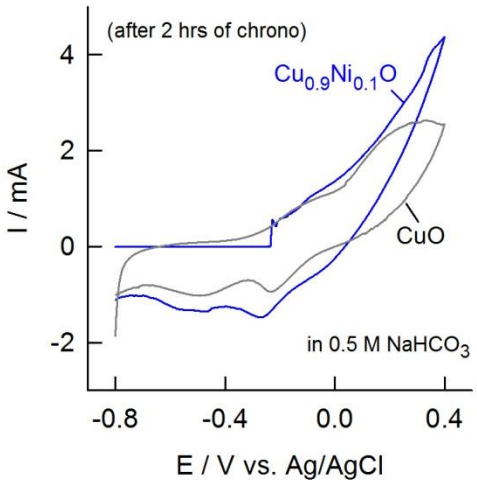

Figure S9. CV of CuO and $Cu_{0.9}Ni_{0.1}O$ post chronoamperometry at -0.8 V for 2 hours. Behavior depicts the formation of metallic copper.

Figure S10

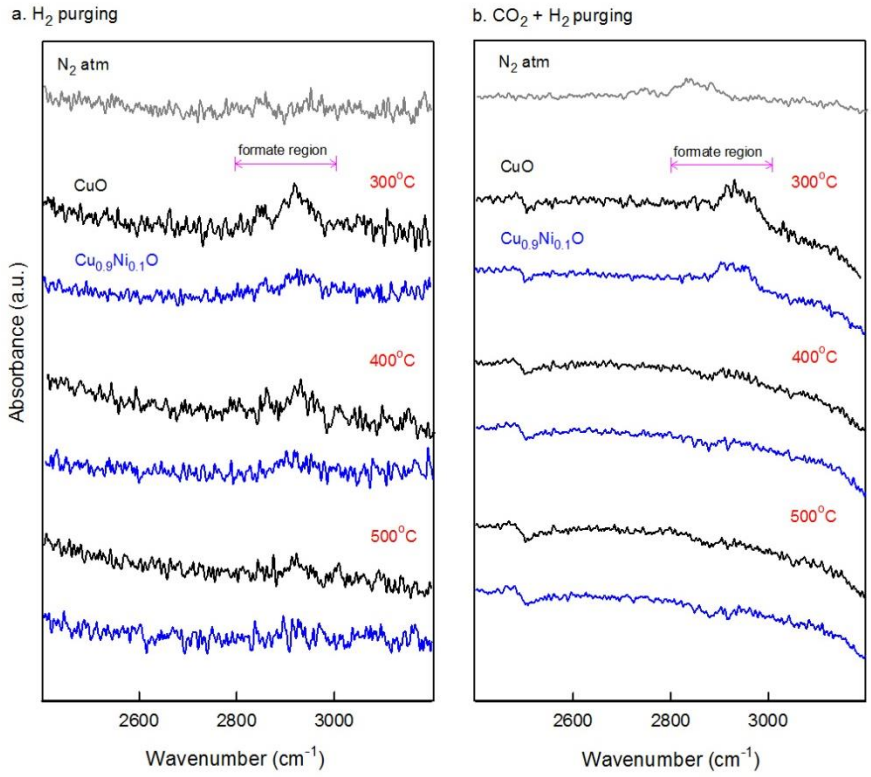

Figure S10. DRIFT spectra recorded in IR ranges (2400 to 3200 cm^{-1}) on passing H_2 (a) and CO_2+H_2 UHP gases (b) over KBr mixed $Cu_{0.9}Ni_{0.1}O$ and CuO catalysts at different temperatures from 300 to 500°C.

Figure S11

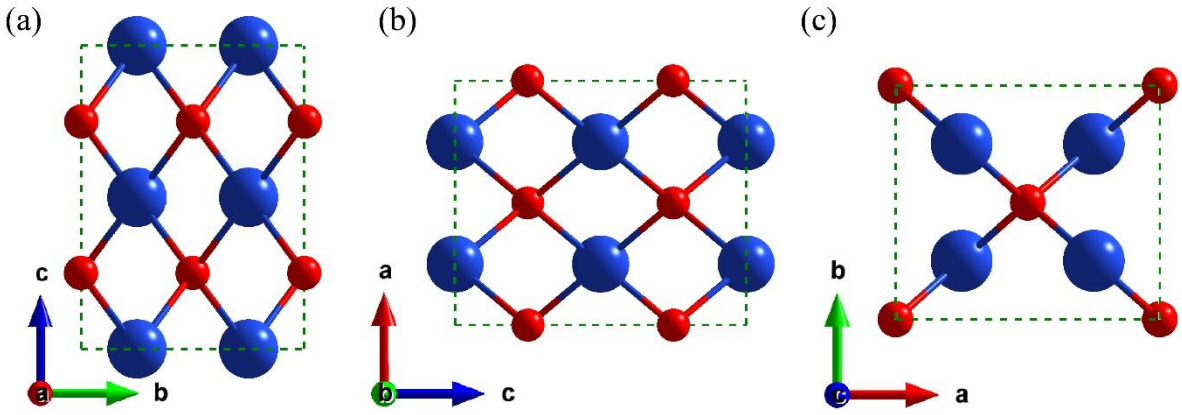

Figure S11. Structures of optimized bulk CuO in a (a), b (b), and c (c) directions, respectively. The blue and red spheres represent Cu, and O atoms, respectively.

Figure S12

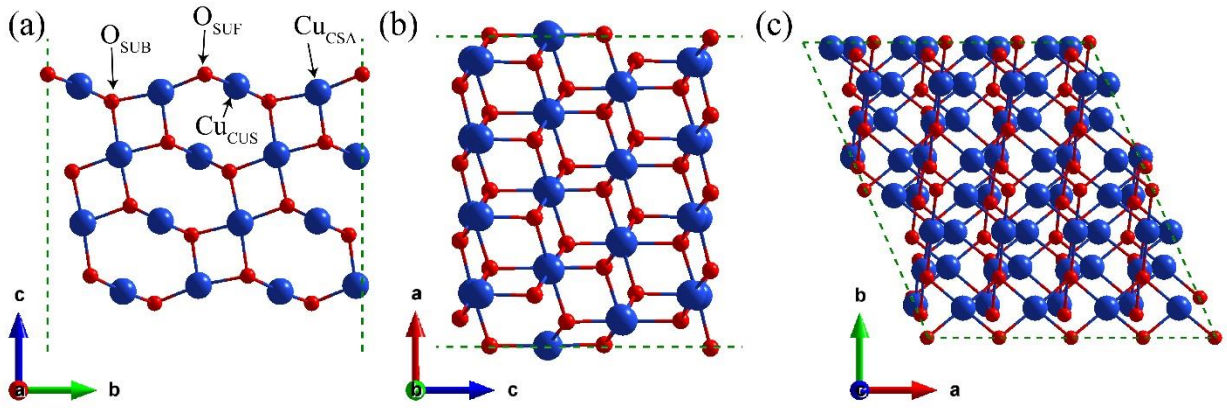

Figure S12. Structures of optimized (111) surface of CuO slab in a (a), b (b), and c (c) directions, respectively. The blue and red spheres represent Cu and O atoms, respectively.

Figure S13

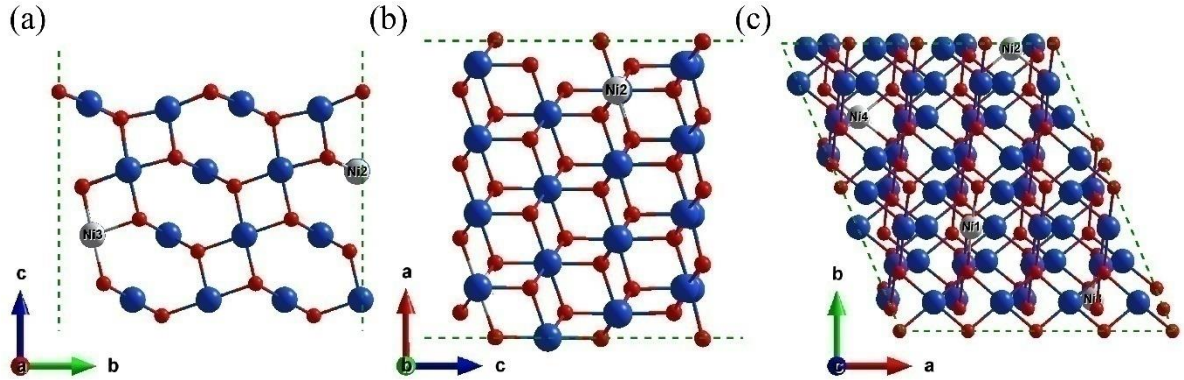

Figure S13. Structures of optimized (111) surface of $Cu_{0.9375}Ni_{0.0625}O$ slab in a (a), b (b), and c (c) directions, respectively. The blue, red, and grey spheres represent Cu, O, and Ni atoms, respectively.

The adsorption energies of 7 intermediates involved in the CO_2 electro-reduction are calculated according to the following expressions:

$$E_{ads}^{DFT}(COOH) = E(CO_2^*) - [E^* + E(CO_2) + 0.5E(H_2)] \quad (S1)$$

$$E_{ads}^{DFT}(CO) = E(CO^*) - [E^* + E(CO)] \quad (S2)$$

$$E_{ads}^{DFT}(CHO) = E(CHO^*) - [E^* + E(CO) + 0.5E(H_2)] \quad (S3)$$

$$E_{ads}^{DFT}(CH_2O) = E(CH_2O^*) - [E^* + E(CO) + E(H_2)] \quad (S4)$$

$$E_{ads}^{DFT}(CH_3O) = E(CH_3O^*) - [E^* + E(CO) + 1.5E(H_2)] \quad (S5)$$

$$E_{ads}^{DFT}(O) = E(O^*) - [E^* + 0.5E(O_2)] \quad (S6)$$

$$E_{ads}^{DFT}(OH) = E(O^*) - [E^* + E(H_2O) - 0.5E(H_2)] \quad (S7)$$

Figure S14

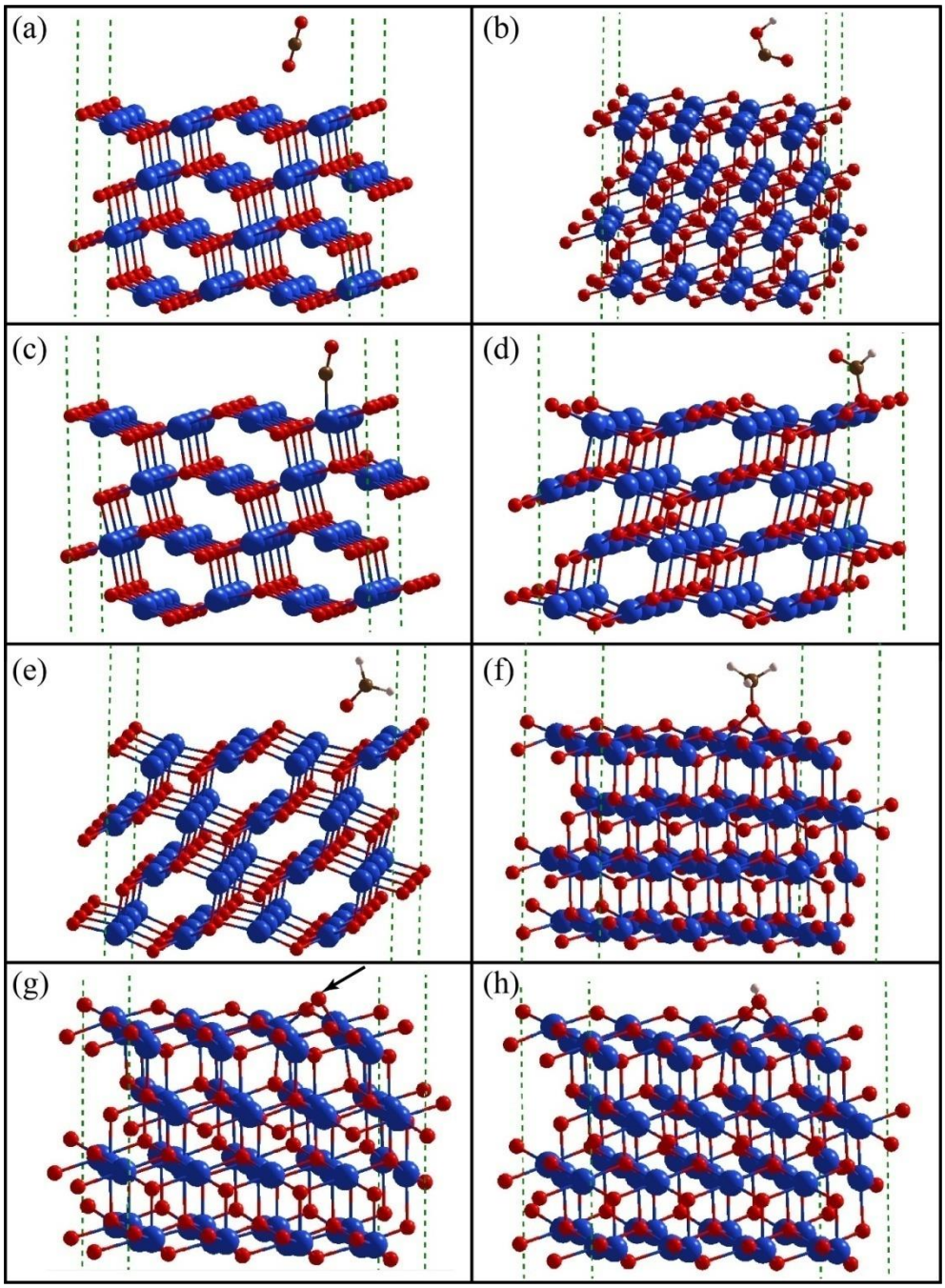

Figure S14. Completely optimized structures of CO_2 (a), COOH (b), CO (c), CHO (d), CH_2O (d), CH_3O (e), O (shown by black arrow) (f), and OH (d) intermediates on (111) surface of CuO. The blue, red, brown, and light pink spheres represent Cu, O, C, and H atoms, respectively.

Figure S15

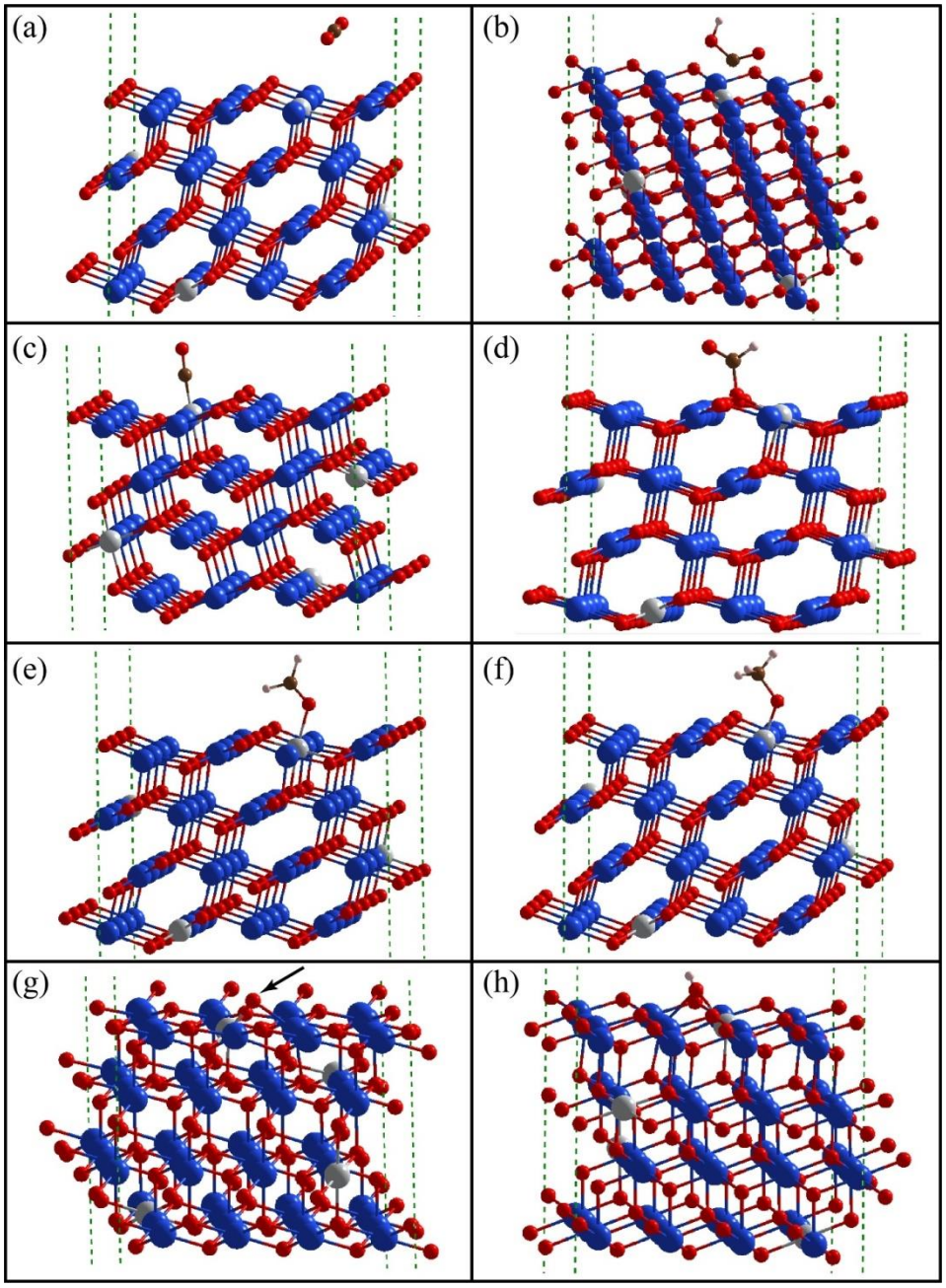

Figure S15. Completely optimized structures of CO_2 (a), COOH (b), CO (c), CHO (d), CH_2O (d), CH_3O (e), O (f), and OH (d) intermediates on (111) surface of $Cu_{0.9375}Ni_{0.0625}O$. The blue, red, grey, brown, and light pink spheres represent Cu, O, Ni, C, and H atoms, respectively.

Figure S16

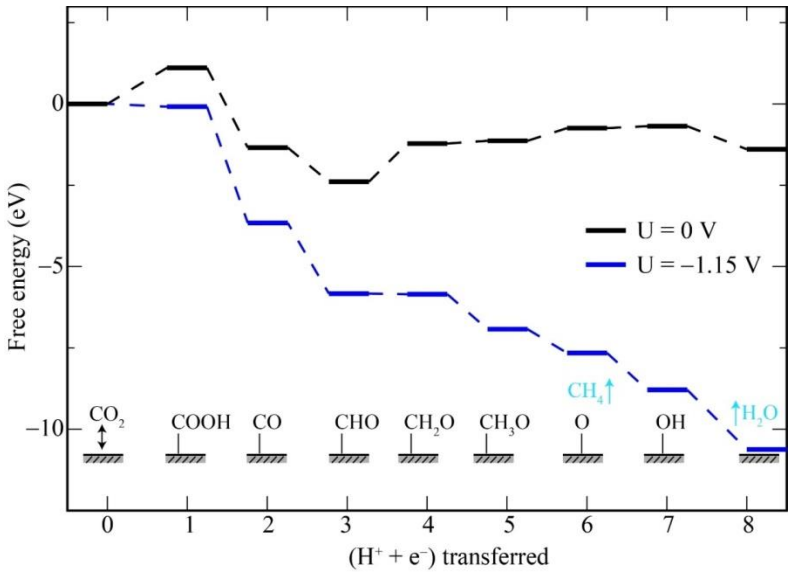

Figure S16. Free energy diagram for electroreduction of CO_2 to CH_4 on (111) surface of CuO.

Table S1. Rietveld refined structural parameters for CuO, $Cu_{0.95}Ni_{0.05}O$ and $Cu_{0.90}Ni_{0.10}O$ compounds.

Compounds	**CuO**	**$Cu_{0.95}Ni_{0.05}O$**	**$Cu_{0.90}Ni_{0.10}O$**
Crystal System	Monoclinic	Monoclinic	Monoclinic
Space group	*C 1 2/c 1* (No. 15)	*C 1 2/c 1* (No. 15)	*C 1 2/c 1* (No. 15)
Lattice Parameters (Å)			
a	4.687(7)	4.682(8)	4.683(7)
b	3.431(4)	3.429(5)	3.429(9)
c	5.136(7)	5.131(9)	5.132(8)
Cell volume ($Å^3$)	81.52(2)	81.30(3)	81.33(4)
β (°)	99.36(4)	99.28(7)	99.27(5)
$R_{Factors}$			
R_{Bragg}	2.52	6.22	8.05
R_F	2.55	6.82	8.01

Table S2. Comparative electrocatalytic performance of the catalyst: Current values are taken from CVs towards for CO_2 electroreduction reaction. BET surface area is used for normalization.

Catalyst	**Current (mA)**	**Current density (mA cm^{-2})**
CuO	0.10	0.063
$Cu_{0.95}Ni_{0.05}O$	0.18	0.360
$Cu_{0.9}Ni_{0.1}O$	0.29	0.400
Ni/CuO	0.06	0.012
NiO/CuO	0.13	0.026

Table S3. Comparative electrocatalytic performance of $Cu_{0.90}Ni_{0.10}O$ catalyst with other copper based electrocatalysts

S.No	Electrocatalyst	Electrolyte	Applied potentials	Products (FE%)	Total
1	Polycrystalline Cu[1]	0.1 M $KHCO_3$	-1.05 V_{RHE}	CH_4 (24.4); C_2H_4 (26.0), CO (1.1) H_2(23.0), C_2H_5OH (9.8), HCOOH (2.1)	91.2%
2	Cu nanoparticles[2]	0.1 M $KClO_4$	-1.1 V_{RHE}	CH_4 (1), C_2H_4 (36), CO (34)	72.0%
3	Cu nano particles[3]	0.1 M $NaHCO_3$	-1.25 V_{RHE}	CH_4 (80%); H_2 (13%)	93.0%
4	Cu nanoflower[4]	0.1 M $KHCO_3$	-1.6 V_{RHE}	CH_4 (5); C_2H_4 (10); H_2 (29); HCOOH (49)	94.0%
5	Au_3Cu[5]	0.1 M $KHCO_3$	-0.73 V_{RHE}	CO (64.7), HCOOH (3.1)	67.8%
6	CuIn[6]	0.1 M $KHCO_3$	-0.6 V_{RHE}	CO (38), HCOOH (34)	72.0%
7	Oxide derived Cu[7]	0.5 M $NaHCO_3$	-0.5 V_{RHE}	CO (40), HCOOH (33)	73.0%
8	Oxide derived Cu foam[8]	0.5 M $NaHCO_3$	-1.0 V_{RHE}	CO (5), HCOOH (5), C_2H_4 (20); C_2H_6 (25)	55.0%
9	Cu/SnO_2[9]	0.5 M $KHCO_3$	-0.7 V_{RHE}	CO (93)	93.0%
10	Cu_2O[10]	0.5 M $KHCO_3$	-1.82 $V_{Ag/AgCl}$	CO (6), CH_4 (1), C_2H_4 (26), HCOOH (8)	41.0%
11	Cu_2O[11]	0.1 M $KHCO_3$	-1.1 V_{RHE}	CO (3), CH_4 (4), C_2H_4 (33), C_2H_6 (9), HCOOH (22)	71.0%
12	CuO nanoparticles[12]	0.2 M $KHCO_3$	-1.7 V_{SCE}	C_2H_5OH (15.5), n-propanol (3.6)	19.1%
		0.2 M KI		C_2H_5OH (36.1), n-propanol (3)	39.1%
13	**$Cu_{0.9}Ni_{0.1}O$**	**0.5 M $NaHCO_3$**	**-0.8 $V_{Ag/AgCl}$** (-0.2 V_{RHE})	**CO (<1), CH_4 (29.4), C_2H_4 (12.9), H_2 (25.4) C_2H_5OH (15.3)**	**83.0%**

RHE-reversible hydrogen electrode; SCE-standard calomel electrode; Ag/AgCl-Silver/Silver chloride electrode

Table S4. DFT energies (E^{DFT}), corrections to free energy (ZPE – TS)[13], and free energies of adsorption (G) of isolated adsorbates which are used as reference for calculating reaction free energies

Species	**E^{DFT}(eV)**	**ZPE– TS[13](eV)**	**G (eV)**
CO_2	-22.95	-0.34	-23.29
CO	-14.77	-0.53	-15.30
H_2O	-14.22	-0.07	-14.29
H_2	-6.77	-0.15	-6.92
O_2	-9.86	-0.19	-10.05

Table S5. DFT adsorption energies (E_{ads}^{DFT}), corrections to free energy (ZPE – TS), and free energies of adsorption (G*) of intermediates on (111) surface of CuO

Intermediates	**E_{ads}^{DFT}(eV)**	**ZPE – TS(eV)**	**G* (eV)**
*COOH	0.35	0.31	1.07
*CO	-1.85	-0.03	-1.35
*CHO	-3.35	0.38	-2.36
*CH_2O	-2.34	0.46	-1.20
*CH_3O	-2.82	0.92	-1.15
*O	-0.83	0.02	-0.72
*OH	-0.99	0.31	-0.69

Table S6. DFT adsorption energies (E_{ads}^{DFT}), corrections to free energy (ZPE – TS), and free energies of intermediates (G*) on (111) surface of $Cu_{0.9375}Ni_{0.0625}O$

Intermediates	E_{ads}^{DFT} **(eV)**	**ZPE – TS(eV)**	**G* (eV)**
*COOH	-1.06	0.45	-0.20
*CO	-0.85	0.06	-0.26
*CHO	-3.12	0.36	-2.15
*CH_2O	-2.64	0.63	-1.33
*CH_3O	-2.77	0.93	-1.09
*O	-0.63	0.02	-0.52
*OH	-0.71	0.30	-0.42

REFERENCES (supp info)

(1) Kuhl, K. P.; Cave, E. R.; Abram, D. N.; Jaramillo, T. F. New Insights into the Electrochemical Reduction of Carbon Dioxide on Metallic Copper Surfaces. *Energy Environ. Sci.* **2012,** *5* (5), 7050-7059.

(2) Tang, W.; Peterson, A. A.; Varela, A. S.; Jovanov, Z. P.; Bech, L.; Durand, W. J.; Dahl, S.; Norskov, J. K.; Chorkendorff, I. The Importance of Surface Morphology in Controlling the Selectivity of Polycrystalline Copper for CO_2 Electroreduction. *Phys. Chem. Chem. Phys.* **2012,** *14* (1), 76-81.

(3) Manthiram, K.; Beberwyck, B. J.; Alivisatos, A. P. Enhanced Electrochemical Methanation of Carbon Dioxide with a Dispersible Nanoscale Copper Catalyst. *J. Am. Chem. Soc.* **2014,** *136* (38), 13319-13325.

(4) Xie, J.-F.; Huang, Y.-X.; Li, W.-W.; Song, X.-N.; Xiong, L.; Yu, H.-Q. Efficient Electrochemical CO_2 Reduction on a Unique Chrysanthemum-like Cu Nanoflower Electrode and Direct Observation of Carbon Deposite. *Electrochim. Acta* **2014,** *139*, 137-144.

(5) Kim, D.; Resasco, J.; Yu, Y.; Asiri, A. M.; Yang, P. Synergistic Geometric and Electronic Effects for Electrochemical Reduction of Carbon Dioxide Using Gold-Copper Bimetallic Nanoparticles. *Nature Communi.* **2014,** *5*, 4948-4956.

(6) Rasul, S.; Anjum, D. H.; Jedidi, A.; Minenkov, Y.; Cavallo, L.; Takanabe, K. A Highly Selective Copper-Indium Bimetallic Electrocatalyst for the Electrochemical Reduction of Aqueous CO_2 to CO. *Angew. Chem. Int. Ed. Engl.* **2015,** *54* (7), 2146-2150.

(7) Li, C. W.; Kanan, M. W. CO_2Reduction at Low Overpotential on Cu Electrodes Resulting from the Reduction of Thick Cu_2O Films. *J. Am. Chem. Soc.* **2012,** *134* (17), 7231-7234.

(8) Dutta, A.; Rahaman, M.; Luedi, N. C.; Mohos, M.; Broekmann, P. Morphology Matters: Tuning the Product Distribution of CO_2 Electroreduction on Oxide-Derived Cu Foam Catalysts. *ACS Catal.* **2016,** *6* (6), 3804-3814.

(9) Li, Q.; Fu, J.; Zhu, W.; Chen, Z.; Shen, B.; Wu, L.; Xi, Z.; Wang, T.; Lu, G.; Zhu, J. J.; Sun, S. Tuning Sn-Catalysis for Electrochemical Reduction of CO_2 to CO via the Core/Shell Cu/SnO_2 Structure. *J. Am. Chem. Soc.* **2017,** *139* (12), 4290-4293.

(10) Kim., D.; Lee., S.; Ocon., J. D.; Jeong., B.; Leeb., J. K.; Lee., J. Insights into an Autonomously Formed Oxygen-evacuated Cu_2O Electrode for the Selective Production of C_2H_4 from CO_2. *Phys. Chem. Chem. Phys.* **2015,** *17*, 824-830.

(11) Kas, R.; Kortlever, R.; Milbrat, A.; Koper, M. T.; Mul, G.; Baltrusaitis, J. Electrochemical CO_2 Reduction on Cu_2O-derived Copper Nanoparticles: Controlling the Catalytic Selectivity of Hydrocarbons. *Phys. Chem. Chem. Phys.* **2014,** *16* (24), 12194-12201.

(12) Chi., D.; Yang., H.; Du., Y.; Lv., T.; Sui., G.; Wang., H.; Lu, J. Morphology-Controlled CuO Nanoparticles for Electroreduction of CO_2 to Ethanol. *RSC Adv.* **2014,** *4*, 37329–37332.

(13) Peterson, A. A.; Abild-Pedersen, F.; Studt, F.; Rossmeisl, J.; Norskov, J.K.; How Copper Catalyzes the Electroreduction of Carbon Dioxide into Hydrocarbon Fuels. *Energy Environ. Sci.* **2010**, 3, 1311-1315.

*****